Journal of Hyperbolic Differential Equations
Vol. 7, No. 3 (2010) 383–404

DOI: 10.1142/S0219891610002177

World Scientific
www.worldscientific.com

ENTROPY CONSERVATIVE SCHEMES AND ADAPTIVE MESH SELECTION FOR HYPERBOLIC CONSERVATION LAWS

CHRISTOS ARVANITIS* and CHARALAMBOS MAKRIDAKIS*,†

*Department of Applied Mathematics
University of Crete, 71409 Heraklion-Crete, Greece

†Institute of Applied and Computational Mathematics
FO.R.T.H. Heraklion, 71110, Greece

NIKOLAOS I. SFAKIANAKIS

Department of Mathematics
University of Vienna, 1090 Vienna, Austria

Received 21 Aug. 2009
Accepted 15 Jun. 2010

Communicated by P. G. LeFloch

Abstract. We consider numerical schemes which combine non-uniform, adaptively redefined spatial meshes with entropy conservative schemes for the evolution step for shock computations. We observe that the resulting adaptive schemes yield approximations free of oscillations in contrast to known fully discrete entropy conservative schemes on uniform meshes. We conclude that entropy conservative schemes are transformed to *entropy diminishing* schemes when combined with the proposed geometrically driven mesh adaptivity.

Keywords: Adaptive mesh refinement; entropy conservative schemes; non-classical shocks.

Mathematics Subject Classification 2010: 65M50

1. Introduction

We consider scalar conservation laws in one space dimension,

$$u_t + f(u)_x = 0, \quad x \in [a, b], \quad t \in [0, T], \tag{1.1}$$

with initial data u_0 having compact support in a much smaller interval.

We are interested in studying numerical approximations of the exact solution u of (1.1) over *non-uniform, adaptively redefined* spatial meshes. Adaptivity is a main theme in modern scientific computing of complex physical phenomena. It is therefore important to investigate the behavior of adaptive schemes for hyperbolic

problems, such as (1.1), which exhibit several interesting and not trivial characteristics. In this work, we investigate the behavior of certain geometrically driven adaptive algorithms when combined with the important class of entropy conservative schemes of Tadmor.

The adaptive schemes we will consider have the following structure: in every time step $t = t^n$ the mesh that we consider is:

$$M_x^n = \{a = x_1^n < \cdots < x_N^n = b\}$$

with variable space step sizes $h_i^n = x_{i+1}^n - x_i^n$, $i = 1, \ldots, N-1$. We note moreover, that the mesh is reconstructed in every time step. We consider also numerical approximations U^n of the exact solution u over the mesh M_x^n at time $t = t^n$ with

$$U^n = \{U_1^n, \ldots, U_N^n\}.$$

The creation and manipulation of such non-uniform meshes and the time evolution of the approximate solutions is dictated by the Main Adaptive Scheme (MAS) which in short is described by the following procedures

- In every time step, construct new mesh/space;
- Update numerical approximations over the new space;
- Evolve in time with the numerical scheme.

In the next section, we shall discuss in detail the main adaptive scheme, we just note here that we use a fixed number of spatial nodes and that the mesh reconstruction procedure is based on information attained by the geometry of the numerical approximation itself.

Applications of the main adaptive scheme on several problems, point out a strong stabilization property emanating from the mesh reconstruction [1, 3, 14]. This stabilization property led us to combine MAS with the marginal class of entropy conservative schemes. Entropy conservative schemes were first introduced by Tadmor [15] and further studied by LeFloch and Rhode [12], Tadmor [16], Lukáčová-Medvi̇ďová and Tadmor [13]. They are semi-discrete numerical schemes which satisfy an exact entropy equality. On one hand these schemes are interesting on their own right, for they appear in the context of zero dispersion limits, complete integrable systems and computation of non-classical shocks. On the other hand, they are important as building blocks for the construction of entropy stable schemes [13, 15, 16]. Out of their properties we shall focus on the following: explicit in time discretization of the entropy conservative schemes leads to entropy production and numerical instabilities occur in the form of oscillations [16].

The aim of this work is to combine the main adaptive scheme with entropy conservative schemes for the evolution step. We note in advance that the stabilization properties of MAS are able to tame out the oscillations produced by the fully discrete entropy conservative schemes; hence we conclude that the entropy dissipation due to proper mesh reconstruction counterbalances the entropy production due to explicit in time discretization. In other words the main conclusion of this work is

that entropy conservative schemes are transformed to *entropy diminishing* schemes when combined with the geometrically driven mesh redistribution of Sec. 2.

This work is divided in the following sections, in Sec. 2, we present the MAS and give some details regarding the steps and the implementation of this scheme. In Sec. 3, we are following [15, 16] and we briefly overview the notion of *entropy variables* and the construction of entropy conservative semi-discrete schemes. In Sec. 4, we investigate the computational behavior of the schemes by considering several numerical tests/problems suggested in [12, 16]. In each problem, we construct the respective semi-discrete schemes and discuss on their fully discrete versions. We shall witness, as mentioned above, that the combination of MAS with fully discrete, explicit in time entropy conservative schemes, tames out oscillations. In addition, the application of adaptivity to entropy conservative schemes designed to capture non-classical behavior lead to approximations of similar type to entropy diminishing schemes. Thus, adaptive entropy conservative schemes fail on resolving non-classical shocks.

2. The Main Adaptive Scheme

We focus in this section on the study of the Main Adaptive Scheme (MAS) and its properties. To start with, we note that in the uniform mesh case the evolution of the numerical approximations is dictated solely by the numerical scheme under consideration. In the contrary, in the non-uniform case, the scheme consists of *three intermediate procedures* in each time step. These comprise the Main Adaptive Scheme (MAS).

Definition 2.1 (MAS). Given mesh $M_x^n = \{a = x_1^n < \cdots < x_N^n = b\}$ and approximations $U^n = \{U_1^n, \ldots, U_N^n\}$,

Step 1. (Mesh reconstruction)
Construct new mesh $M_x^{n+1} = \{a = x_1^{n+1} < \cdots < x_N^{n+1} = b\}$.

Step 2. (Solution update)
Given M_x^n, U^n and M_x^{n+1}

2a. construct a function $V^n(x)$ such that $V^n(x_i^n) = U_i^n$;

2b. compute/update approximations $\hat{U}^n = \{\hat{U}_1^n, \ldots, \hat{U}_N^n\}$ over M_x^{n+1}.

Step 3. (Time evolution)
Given M_x^{n+1}, $\hat{U}^n$ march in time to compute $U^{n+1} = \{U_1^{n+1}, \ldots, U_N^{n+1}\}$.

A first comment is that in the uniform mesh case the mesh does not change with time so there is no need for mesh reconstruction M_x^{n+1} (no Step 1); hence there is no need for solution update (no Step 2). In this case the MAS (Definition 2.1) reduces to time evolution step (Step 3) which is just the the usual numerical scheme over a uniform mesh. The extra steps of the non-uniform MAS on one hand change significantly both the computation and the analysis of the numerical approximations U^n and on the other hand, under conditions, are responsible for stabilization properties of the MAS.

The use of non-uniform adaptively redefined meshes, in the context of finite differences, has been studied in the past; we mention for instance the work of Harten and Hyman [9], Dorfi and Drury [6] and Tang and Tang [17], among others. See also [11]. In these works however standard entropy stable schemes were considered.

The approach that we shall follow, for the mesh reconstruction step of MAS (Step 1) was first introduced by Arvanitis, Katsaounis and Makridakis [2] and by Arvanitis [4]. This approach is different in the sense that it utilizes geometric information attained from the numerical solution and redistributes a fixed number of nodes according to an equi-distribution principle. Properties and variations of MAS procedure have been studied later in [1, 3, 5].

We start the discussion of MAS with the mesh reconstruction procedure (Step 1). This procedure is a way of relocating the nodes of the mesh according to the geometric *information* contained in the discrete numerical solution. The basic idea is simple and geometric:

> *in areas where the numerical solution is smoother/flatter the density of the nodes is low, in the contrary in areas where the numerical solution is less smooth/flat the density of the nodes should be higher*

In more detail, at a given time step, the basic principles of the mesh reconstruction procedure (Step 1 of MAS) are:

(a) Locate the regions of space where increased accuracy is demanded, through a positive functional g_{U_h} of the approximate solution U_h.
(b) Find a partition $\{x_n\}_{n=1}^N$ of the space Ω with predefined cardinality N, and density that follows the estimator function g_{U_h}, i.e. the new mesh satisfies the equidistribution principle:

$$\int_{[x_i,x_{i+1}]} g_{U_h} = \frac{1}{N}\int_\Omega g_{U_h}, \quad i = 0, 1, \ldots, N-1.$$

Examples of geometric estimator functions that have been used are the arclength estimator, the gradient estimator and the curvature estimator. For reasons deployed in [4, 5], we use the curvature of the approximate solution as estimator function which, for the case of smooth function U is defined as follows:

$$g_U(x) = \frac{|U''(x)|}{(1+(U'(x))^2)^{\frac{3}{2}}}. \tag{2.1}$$

At the discrete level, given a partition $\{x_i\}_{i=1}^N$, we approximate the curvature $g_{U_h}(x_i)$ of the discrete solution $\{U_{h,i}\}_{i=1}^N$, with $g_{U_h,i}$ given by

$$g_{U_h,i} = \frac{1}{R(A_{i-1}, A_i, A_{i+1})}$$

where $R(A_{i-1}, A_i, A_{i+1})$ is the radius of the circumcircle that passes through the three points $A_j = (x_j, U_{h,j}), j = i-1, i, i+1$, that is

$$g_{U_h,i} = 2\frac{\|(A_{i+1} - A_i) \times (A_i - A_{i-1})\|}{\|A_{i+1} - A_i\| \, \|A_{i+1} - A_{i-1}\| \, \|A_i - A_{i-1}\|}, \quad i = 1, \ldots, N \tag{2.2}$$

For equidistant points A_{i-1}, A_i, A_{i+1}, relation (2.2) is a second order approximation of the curvature (2.1). Closing with the mesh reconstruction step, we note that one can easily prove that the computational cost of constructing a new mesh with this procedure is $\mathcal{O}(N)$, where N is the fixed number of spatial nodes.

We now move to the solution update procedure (Step 2 of MAS). We have an old mesh M_x^n from the initiation of the MAS and a new mesh M_x^{n+1} from the mesh reconstruction procedure (Step 1 of MAS). The approximate solution U^n is defined over the old mesh M_x^n, and we want to redefine the approximate solution over the new mesh M_x^{n+1}.

To this end we consider vertex centered grids. That is, we consider a partition of the domain in cells C_i^n defined as:

$$C_i^n = [x_{i-1/2}^n, \; x_{i+1/2}^n), \quad x_{i+1/2}^n = \frac{x_i^n + x_{i+1}^n}{2}.$$

Over the old set of cells C_i^n we construct the piecewise constant function $V^n(x)$ that satisfies $V^n(x_i^n) = U_i^n$.

The set of cells C_i^n is defined through the old mesh M_x^n. Similarly we consider a new set of cells C_i^{n+1} defined through the new mesh M_x^{n+1} as follows:

$$C_i^{n+1} = [x_{i-1/2}^{n+1}, \; x_{i+1/2}^{n+1}), \quad x_{i+1/2}^{n+1} = \frac{x_i^n + x_{i+1}^{n+1}}{2}.$$

Now we can compute the updated values $\hat{U}^n = \{\hat{U}_1^n, \ldots, \hat{U}_N^n\}$ in a mass conservative way [1].

Definition 2.2 (Conservative construction of $\hat{U}^n$). We take into account the configuration of the new nodes x_i^{n+1} with respect to the old cells C_i^n. So we have the following cases:

- If the configuration of the new nodes x_{i-1}^{n+1}, x_i^{n+1}, x_{i+1}^{n+1} is such that

$$x_{i-1/2}^{n+1} \in C_k^n \quad \text{and} \quad x_{i+1/2}^{n+1} \in C_l^n, \quad \text{with } k < l,$$

  we define

$$\hat{u}_i^n = \frac{1}{\Delta x_i^{n+1}} \left((x_{k+1/2}^n - x_{i-1/2}^{n+1}) u_k^n + \sum_{j=k+1}^{l-1} \Delta x_j^n u_j^n + (x_{i+1/2}^{n+1} - x_{l-1/2}^n) u_l^n \right).$$

- If the configuration of the new nodes x_{i-1}^{n+1}, x_i^{n+1}, x_{i+1}^{n+1} is such that

$$x_{i-1/2}^{n+1}, \; x_{i+1/2}^{n+1} \in C_k^n,$$

we define

$$\hat{u}_i^n = u_k^n.$$

This construction is conservative, respects the maximum principle and is of linear complexity with respect to the fixed number of nodes N.

Proposition 2.3. *The construction defined in Definition 2.2 is conservative.*

Proof. The area defined by the new approximation $\hat{u}_i^n$, over the new cell C_i^{n+1}, is

$$\hat{u}_i^n \Delta x_i^{n+1} = (x_{k+1/2}^n - x_{i-1/2}^{n+1})u_k^n + \sum_{j=k+1}^{l-1} \Delta x_j^n u_j^n + \underbrace{(x_{i+1/2}^{n+1} - x_{l-1/2}^n)u_l^n}_{A}.$$

We write the following term

$$\hat{u}_{i+1}^n \Delta x_{i+1}^{n+1} = \underbrace{(x_{l+1/2}^n - x_{i+1/2}^{n+1})u_l^n}_{B} + \sum_{j=l+1}^{m-1} \Delta x_j^n u_j^n + (x_{i+3/2}^{n+1} - x_{m-1/2}^n)u_m^n$$

and sum with the previous one $\hat{u}_i^n \Delta x_i^{n+1}$. We we notice that the terms A and B merge with the existing sums and we end up with the following right-hand side

$$(x_{k+1/2}^n - x_{i-1/2}^{n+1})u_k^n + \sum_{j=k+1}^{m-1} \Delta x_j^n u_j^n + (x_{i+3/2}^{n+1} - x_{m-1/2}^n)u_m^n,$$

which is sufficient for conservation. □

We can also prove that this construction of $\hat{U}^n$ respects the maximum principle.

Proposition 2.4 (Maximum principle). *The values of the new point approximations $\hat{u}_i^n$ are bounded by the maximum of the old point approximations u_i^n,*

$$\max_i |\hat{u}_i^n| \leq \max_i |u_i^n|.$$

Proof. In the case where the configuration of the new nodes x_{i-1}^{n+1}, x_i^{n+1}, x_{i+1}^{n+1} is such that

$$x_{i-1/2}^{n+1} \in C_k^n \quad \text{and} \quad x_{i+1/2}^{n+1} \in C_l^n, \quad \text{with } k < l,$$

the new approximation $\hat{u}_i^n$ is defined as

$$\hat{u}_i^n = \frac{1}{\Delta x_i^{n+1}} \left((x_{k+1/2}^n - x_{i-1/2}^{n+1})u_k^n + \sum_{j=k+1}^{l-1} \Delta x_j^n u_j^n + (x_{i+1/2}^{n+1} - x_{l-1/2}^n)u_l^n \right).$$

Since the intervals in the enumerator of the right-hand side sum up to Δx_i^{n+1} we immediately bound as follows

$$|\hat{u}_i^n| \leq \max\{|u_j^n|, j = k, \ldots, l\}.$$

In the case where the configuration of the new nodes x_{i-1}^{n+1}, x_i^{n+1}, x_{i+1}^{n+1} is such that

$$x_{i-1/2}^{n+1},\ x_{i+1/2}^{n+1} \in C_k^n,$$

the new approximation $\hat{u}_i^n$ is defined as

$$\hat{u}_i^n = u_k^n,$$

so again the bound

$$|\hat{u}_i^n| \leq \max\{|u_j^n|, j = k, \ldots, l\}$$

is valid. □

Finally, for the time evolution procedure (Step 3 of MAS), we use any numerical scheme valid for non-uniform meshes. The numerical schemes that we consider in this work are explicit (in time) discretizations of entropy conservative schemes.

3. Entropy Conservative Schemes

In this paragraph, we present a short overview of the construction of entropy conservative schemes following [15, 16]. We will restrict our attention to the construction of 3-point second order accurate schemes. The construction starts by assuming that the one dimensional conservation law

$$u_t + f(u)_x = 0$$

— with f a smooth, convex flux function — is equipped with a convex entropy function $U(u)$ along with an entropy flux function F, which satisfies

$$F'(u) = U'(u)f'(u).$$

Remark 3.1. The entropy function U is not to be confused with the numerical approximations U^n since for the later we shall always use a superscript.

The entropy function U provides the new variables — the entropy variables [7, 8],

$$v(u) = U'(u),$$

and due to the convexity of U the mapping $u(v)$ is 1-1; hence it serves as a change of variables $u = u(v)$. With respect to the new variables v, the initial conservation

law yields

$$\frac{\partial}{\partial_t}u(v) + \frac{\partial}{\partial_x}g(v) = 0, \quad g(v) = f(u(v)).$$

The potential functions that follow play an essential role in the construction and analysis of the entropy conservative schemes, namely the entropy potential, $\phi(v)$ is defined as

$$u(v) = \frac{d}{dv}\phi(v), \quad \text{i.e. } \phi(v) = vu(v) - U(u(v)), \tag{3.1}$$

and the entropy flux potential $\psi(v)$ is defined as

$$g(v) = \frac{d}{dv}\psi(v) \quad \text{or} \quad \psi(v) = vg(v) - F(u(v)). \tag{3.2}$$

We can now introduce the entropy conservative numerical flux

$$g_{i+\frac{1}{2}} = \int_{\xi=0}^{1} g(v_i + \xi(v_{i+1} - v_i))d\xi = \frac{\psi(v_{i+1}) - \psi(v_i)}{v_{i+1} - v_i},$$

which provides the entropy conservative centered semi-discrete numerical scheme:

$$\frac{d}{dt}u_i(t) = -\frac{1}{\Delta x_i}(g_{i+\frac{1}{2}} - g_{i-\frac{1}{2}}). \tag{3.3}$$

It is proven in [15, Theorem 4.1] that the semi-discrete scheme (3.3) is in fact entropy conservative.

Remark 3.2. As described by Tadmor in [15], conservative schemes with more numerical viscosity than the entropy conservative ones are entropy stable (Theorem 5.2). Furthermore, conservative schemes containing more viscosity than an entropy stable scheme are also entropy stable (Theorem 5.3). So there is a type of ordering in the class of entropy conservative/stable schemes with the entropy conservative being a marginal class.

The entropy conservative scheme (3.3) are semi-discrete schemes, for the fully discrete numerical scheme, we perform explicit in time discretization, through which the scheme (3.3) recasts into

$$u_i^{n+1} = u_i^n - \frac{\Delta t}{\Delta x_i}(g_{i+\frac{1}{2}} - g_{i-\frac{1}{2}}). \tag{3.4}$$

To justify our choice of explicit time discretization, we refer to [16] to note that implicit time discretization enforces entropy stability, on the contrary explicit time discretization leads to entropy production. The entropy conservative schemes, though, *do not* lead to entropy dissipation; hence there is no counterbalance for the entropy production due to explicit time discretization. This leads to instabilities which numerically are presented in the form of oscillations.

Hence by combining the MAS with entropy conservative schemes for the time evolution (Step 3), we can test the entropy dissipation properties of the mesh reconstruction (Step 1) and the solution update (Step 2) of the MAS.

4. Adaptivity and Numerical Dissipation

We shall discuss four test cases where the entropy dissipation of the MAS is exhibited. The first three are 3-point entropy conservative schemes. We follow the work of Tadmor [15, 16] up to the point of constructing a semi-discrete entropy conservative scheme. Then we use an explicit version of the scheme as the evolution step in our adaptive algorithm.

The final example is a 5-point entropy conservative semi-discrete scheme emanating from the work of LeFloch and Rhode [12] designed to approximate non-classical shocks. The time discretization in this example is a 4th order Runge–Kutta scheme.

In all numerical experiments we studied, we noticed that the adaptive mesh case eliminates the oscillations with optimal CFL condition. In the more interesting examples, we display the results of both uniform and adaptive mesh selection. For the rest we just present the adaptive mesh case, since it is well known that the relevant uniform mesh schemes produce oscillations of large magnitude rather fast.

4.1. *Problem 1*

First example is the inviscid Burgers equation:

$$u_t + \left(\frac{1}{2}u^2\right)_x = 0$$

equipped with entropy function

$$U(u) = -\ln u.$$

We follow the steps stated in the introduction up to the point of constructing the respective semi-discrete entropy conservative scheme. We then select the temporal discretization and create the fully-discrete entropy conservative scheme. In this example, we have $U(u) = -\ln u$ and $F(u) = -u$. By the convexity of the entropy function $U(u)$, we perform the following change of variables

$$v(u) = U'(u) \Rightarrow v(u) = -\frac{1}{u} \Rightarrow u(v) = -\frac{1}{v},$$

the entropy variable flux reads

$$g(v) = f(u(v)) \quad \text{or} \quad g(v) = -\frac{1}{2v^2},$$

and the model equation recasts into

$$\frac{\partial}{\partial_t}u(v) + \frac{\partial}{\partial_x}g(v) = 0.$$

For the spatial discretization, we shall make use of the entropy flux potential $\psi(v)$,

$$\psi(v) = vg(v) - F(u(v)), \quad \text{i.e. } \psi(v) = -\frac{1}{2v},$$

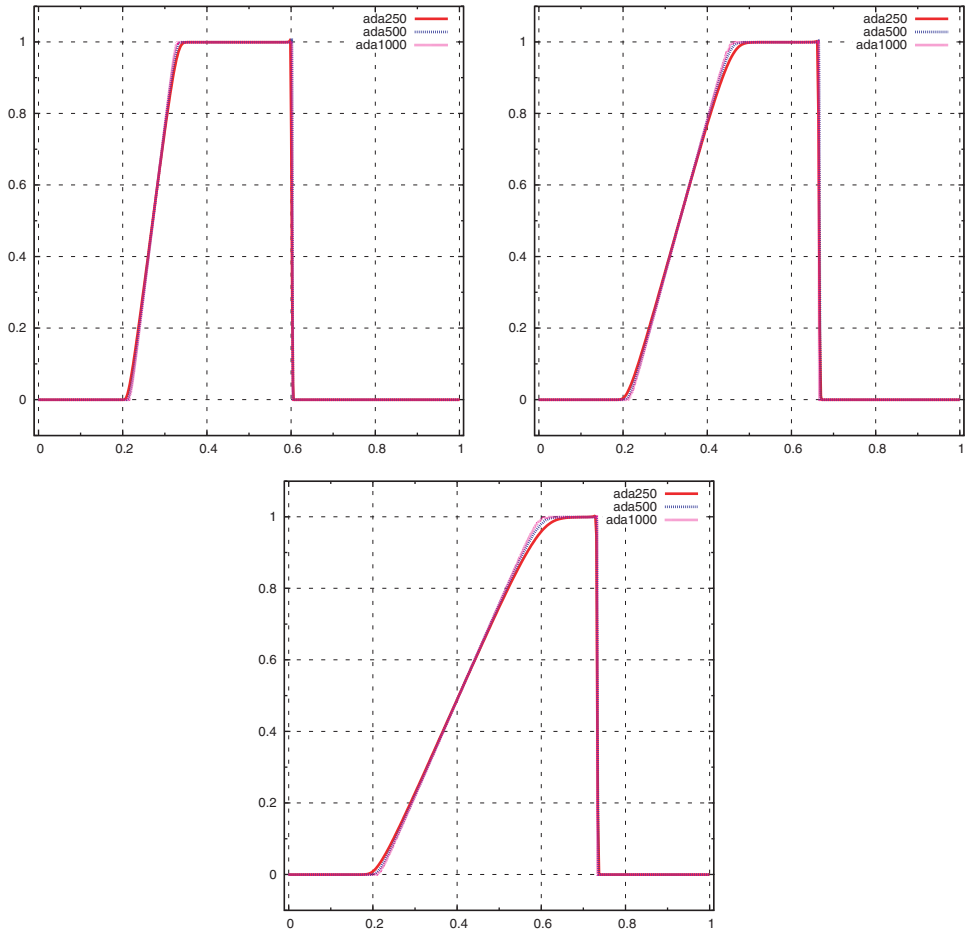

Fig. 1. (Problem 1.) Burgers equation with box initial conditions. The pair entropy/entropy flux considered is $(U(u), F(u)) = (-\ln u, -u)$. We present the numerical solutions for times $t = 0.1$, $t = 0.225$ and $t = 0.375$ only for the non-uniform adaptive case since the uniform exhibits large scale oscillations. In each graph, we present the numerical solutions for $N = 250,\ 500,\ 1000$ cells. We note the lack of oscillations in all three time steps despite the increasing number N of cells.

and the entropy conservative flux shall be

$$g_{i+\frac{1}{2}} = \frac{\psi(v_{i+1}) - \psi(v_i)}{v_{i+1} - v_i} \quad \text{or} \quad g_{i+\frac{1}{2}} = \frac{1}{2}\frac{1}{v_{i+1}v_i} = \frac{1}{2}u_{i+1}u_i.$$

We employ the last result to write the *entropy conservative centered semi-discrete numerical scheme*,

$$\frac{d}{dt}u_i(t) = -\frac{1}{\Delta x_i}(g_{i+\frac{1}{2}} - g_{i-\frac{1}{2}}), \quad \text{i.e. } \frac{d}{dt}u_i(t) = -u_i(t)\frac{u_{i+1}(t) - u_{i-1}(t)}{x_{i+1} - x_{i-1}}.$$

Finally — as we explained earlier — we discretize explicitly in time and the fully discrete scheme is:

$$u_i^{n+1} = u_i^n - \frac{\Delta t}{x_{i+1} - x_{i-1}} u_i^n (u_{i+1}^n - u_{i-1}^n). \tag{4.1}$$

We refer to Fig. 1 for an initial presentation of the adaptive mesh case. The numerical scheme used is (4.1) and the initial condition is a box. The test is performed for a sequence of increasing number of cells. We also refer to Figs. 2 and 3 for more elaborate tests, where we again use the scheme (4.1) but this time with different initial conditions. We test the adaptive mesh case versus the uniform mesh

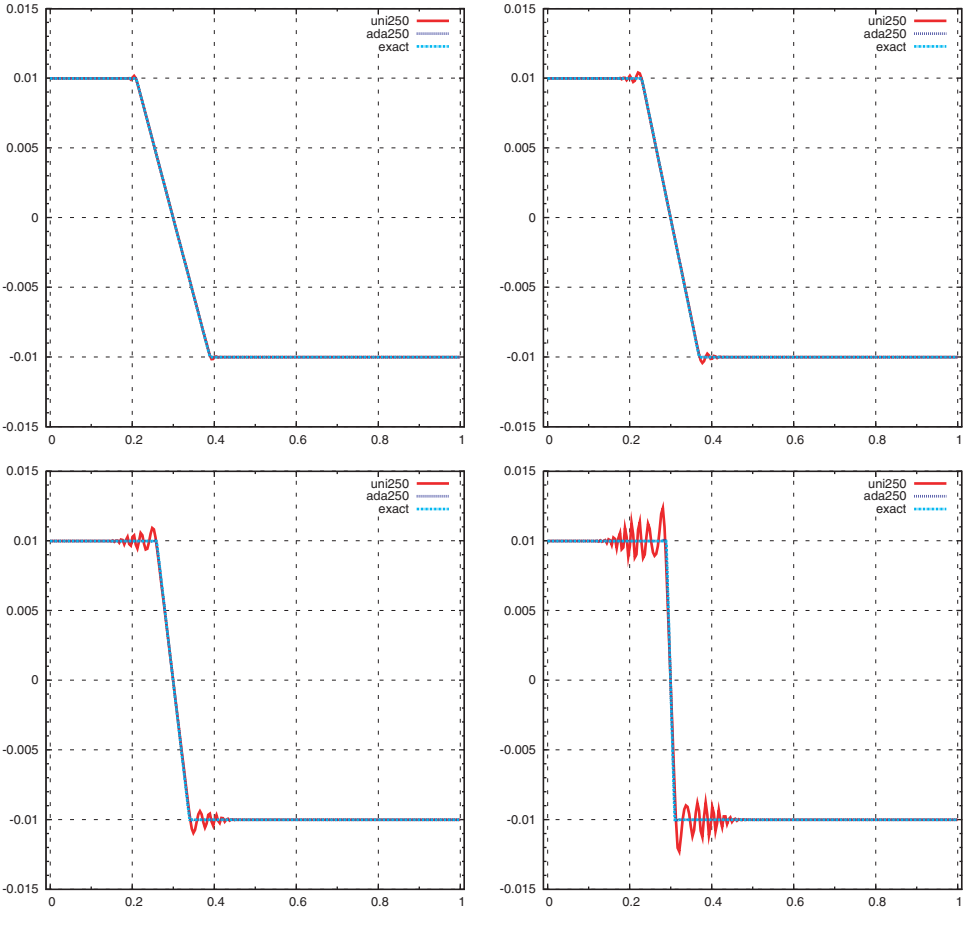

Fig. 2. (Problem 1.) Burgers equation with slow slope initial condition. The pair entropy/entropy flux considered is $(U(u), F(u)) = (-\ln u, -u)$. We exhibit times $t = 1$, $t = 3$, $t = 6$, $t = 9$ for the exact solution, the uniform and the adaptive mesh case. We note that the uniform mesh case exhibits oscillations that rapidly spread to both directions. The adaptive case is clean of oscillations and captures very accurately the exact solution. In this test we utilized $N = 250$ cells and the CFL was set to 0.45.

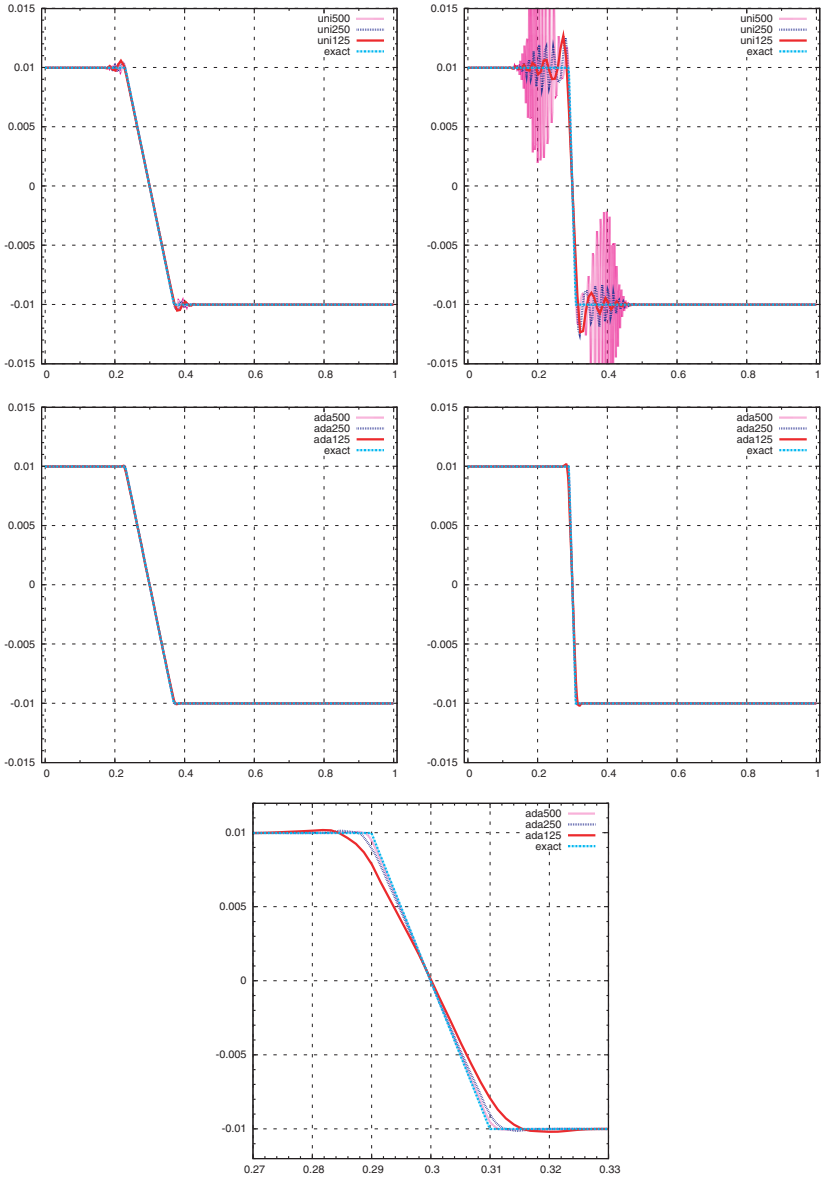

Fig. 3. (Problem 1.) Burgers equation with slow slope initial condition. The pair entropy/entropy flux considered is $(U(u), F(u)) = (-\ln u, -u)$. We exhibit times $t = 3$ and $t = 9$ with increasing number of cells $N = 125$, 250 and 500, separately for the uniform and the adaptive case versus the exact solution of the problem. In the first line, we present the uniform case (left $t = 3$, right $t = 9$) and we note that it exhibits oscillations which grow with respect both to time and to the number of cells N used for the computation. In the second line, we present the adaptive case for the same data (left $t = 3$, right $t = 9$) and we note that the numerical approximations are clean of oscillations and moreover they are indistinguishable from the exact solution in this plotting scale. The graph in the third line is again the adaptive case for $t = 9$ where this time we have focused in the region of the jump, we note here that the limiting profile of the results (as the number of cells N increases) is the exact solution of the problem. For this test the CFL is 0.45.

case and the exact solution of the respective problem. The outcome of these tests is that in the adaptive mesh case oscillations are suppressed and at the same time the exact solution of the problem is resolved accurately.

4.2. *Problem 2*

For the second example we use the same method, 3-point entropy conservative scheme with adaptive mesh selection and explicit time discretization. The convex entropy in this example is $U(u) = e^u$.

In this example the model equation is,

$$u_t + (e^u)_x = 0.$$

The entropy that we want conserved is $U(u) = e^u$ with entropy flux

$$F'(u) = U'(u)f'(u), \quad \text{i.e. } F(u) = \frac{1}{2}e^{2u}.$$

Due to the convexity of the entropy U we perform the following change of variables,

$$v(u) = U'(u) \Rightarrow v(u) = e^u \quad \text{or} \quad u(v) = \ln v.$$

Hence the entropy variables flux reads

$$g(v) = f(u(v)), \quad \text{i.e. } g(v) = v,$$

which provides us with the new model equation

$$\frac{\partial}{\partial_t}u(v) + \frac{\partial}{\partial_x}g(v) = 0.$$

We define the entropy flux potential $\psi(v)$ via,

$$\psi(v) = vg(v) - F(u(v)) \quad \text{or} \quad \psi(v) = \frac{1}{2}v^2.$$

So the entropy conservative flux is written

$$g_{i+\frac{1}{2}} = \frac{\psi(v_{i+1}) - \psi(v_i)}{v_{i+1} - v_i}, \quad \text{i.e. } g_{i+\frac{1}{2}} = \frac{1}{2}(e^{u_{i+1}} + e^{u_i}),$$

and the *entropy conservative centered semi-discrete numerical scheme* reads,

$$\frac{d}{dt}u_i(t) = -\frac{1}{\Delta x_i}(g_{i+\frac{1}{2}} - g_{i-\frac{1}{2}}) \quad \text{hence } \frac{d}{dt}u_i(t) = -\frac{e^{u_{i+1}(t)} - e^{u_{i-1}(t)}}{x_{i+1} - x_{i-1}}.$$

Finally we discretize explicitly in time to get the fully discrete scheme

$$u_i^{n+1} = u_i^n - \frac{\Delta t}{x_{i+1} - x_{i-1}} \cdot (e^{u_{i+1}^n} - e^{u_{i-1}^n}). \tag{4.2}$$

We refer to Fig. 4 for a graphical presentation of a test performed for this scheme over an initial condition that leads to shocks and rarefactions. We compare the

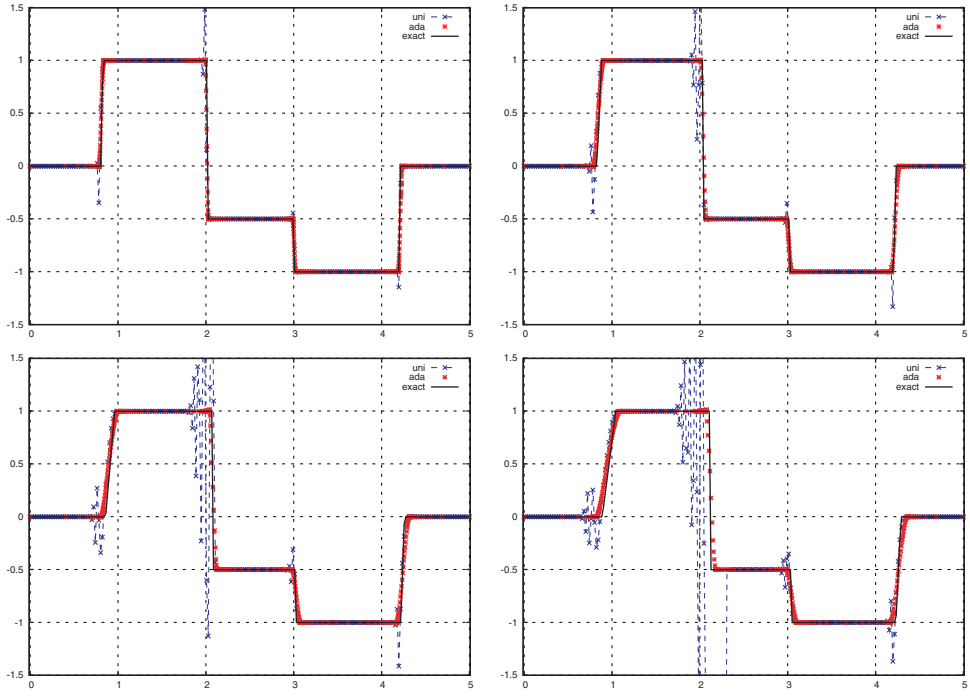

Fig. 4. (Problem 2.) $u_t + (e^u)_x = 0$ with multi shock initial conditions. Entropy/entropy flux $(U(u), F(u)) = (e^u, \frac{1}{2}e^{2u})$. Exhibiting time steps $t = 0.01$, $t = 0.03$, $t = 0.06$, $t = 0.09$ for the exact solution, the uniform and the adaptive mesh case. We note the large amplitude oscillations of the uniform mesh case. The adaptive mesh case is clean and resolves accurately the exact solution. In this example, we utilized a mesh of 250 cells and the CFL was set to 0.3.

adaptive mesh case versus the uniform one versus the exact solution of the problem. As in the previous case the adaptive mesh case is clean of oscillations and resolves the exact solution accurately whereas the uniform one exhibits strong oscillations.

4.3. *Problem 3*

This test is again Burgers equation but this time the entropy is $U(u) = \int^u f(s)ds$. Assuming that u is positive

$$u \geq 0,$$

the entropy U is convex. The choice of the specific entropy function leads to entropy variables flux $g(v) = v$. The work cited in [15, 16] is again used as was previously described.

The model we use is the inviscid Burgers equation:

$$u_t + \left(\frac{1}{2}u^2\right)_x = 0.$$

The entropy we want to conserve in this case is

$$U(u) = \int^u f(s)ds = \int^u \frac{1}{2}s^2 ds = \frac{1}{6}u^3,$$

with entropy flux defined via

$$F'(u) = U'(u)f'(u), \quad \text{i.e. } F(u) = \frac{1}{8}u^4.$$

The convexity of U $(u \geq 0)$ provides us with the new variables v,

$$v(u) = U'(u) \Rightarrow v(u) = \frac{1}{2}u^2 \Rightarrow u(v) = \sqrt{2v}.$$

The entropy variables flux is given by

$$g(v) = f(u(v)) \quad \text{or} \quad g(v) = v,$$

and the new model equation is written as,

$$\frac{\partial}{\partial_t}u(v) + \frac{\partial}{\partial_x}g(v) = 0.$$

We move on to the entropy flux potential $\psi(v)$

$$\psi(v) = vg(v) - F(u(v)), \quad \text{i.e. } \psi(v) = \frac{1}{2}v^2,$$

which provides us with the entropy conservative flux

$$g_{i+\frac{1}{2}} = \frac{\psi(v_{i+1}) - \psi(v_i)}{v_{i+1} - v_i} \quad \text{or} \quad g_{i+\frac{1}{2}} = \frac{1}{4}(u_{i+1}^2 + u_i^2).$$

Hence the *entropy conservative centered semi-discrete numerical scheme* reads

$$\frac{d}{dt}u_i(t) = -\frac{1}{\Delta x_i}(g_{i+\frac{1}{2}} - g_{i-\frac{1}{2}}) \quad \text{hence } \frac{d}{dt}u_i(t) = -\frac{1}{4}\frac{u_{i+1}^2 - u_{i-1}^2}{x_{i+1} - x_{i-1}}.$$

To fully discretize the previous equation we once again use forward Euler time discretization and the fully discrete numerical schemes assumes the form

$$u_i^{n+1} = u_i^n - 0.25\frac{\Delta t}{x_{i+1} - x_{i-1}}(u_{i+1} - u_{i-1})(u_{i+1} + u_{i-1}). \tag{4.3}$$

We refer to Figs. 5 and 6 for a graphical presentations of tests performed for this scheme. More specifically, in Fig. 5, we exhibit a comparison of the adaptive mesh case versus the uniform case where the initial condition is considered to be $u_0(x) = 0.5\sin(2\pi(x + 0.05)) + 0.5$. We witness appearance of oscillations on behalf of the uniform case as soon as the smoothness of the profile is lost, while at the same time the adaptive mesh case remains clean of oscillations. In Fig. 6, we perform tests only for the adaptive mesh case where this time the number of cells N varies. The numerical solutions converge to a sharp limiting profile as the number of cells N increases.

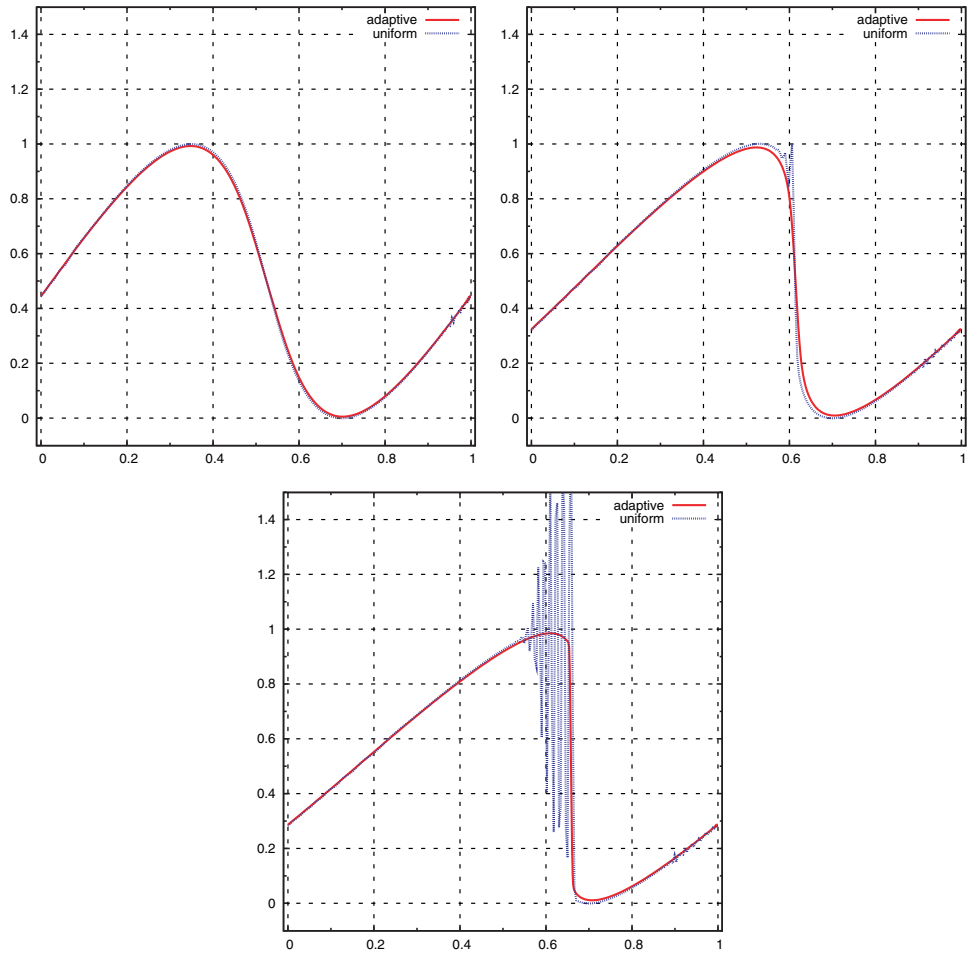

Fig. 5. (Problem 3.) Burgers equation with $u_0(x) = 0.5\sin(2\pi(x + 0.05)) + 0.5$ initial conditions. The pair entropy/entropy flux considered is $(U(u), F(u)) = (\frac{1}{6}u^3, \frac{1}{4}u^4)$. Exhibiting times $t = 0.3$, $t = 0.66$, $t = 0.85$ for the uniform and the adaptive mesh case. We note again the the adaptive mesh case exhibits no oscillations where as in the uniform mesh case they appear as soon as the smoothness of the solution is lost. In this test we used 300 cells and the CFL was set to 0.4.

4.4. *Problem 4*

We now consider a more involved case, namely a 5-point entropy conservative scheme introduced in [12] for approximating non-classical shocks. We consider the one-dimensional model:

$$u_t + (u^3)_x = 0$$

with entropy function

$$U(u) = \int^u f(s)ds \Rightarrow U(u) = \frac{1}{4}u^4.$$

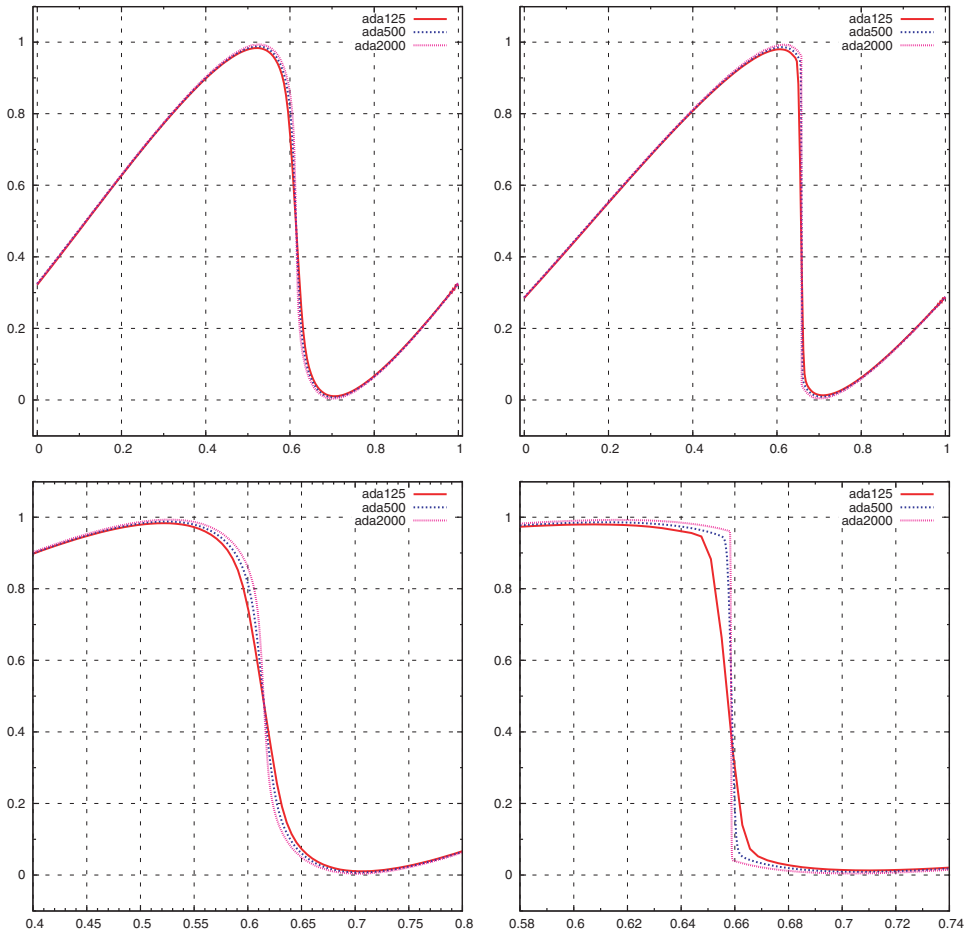

Fig. 6. (Problem 3.) We again consider Burgers equation with $u_0(x) = 0.5\sin(2\pi(x + 0.05)) + 0.5$ initial conditions. The pair entropy/entropy flux considered is $(U(u), F(u)) = (\frac{1}{6}u^3, \frac{1}{4}u^4)$. In this test we present times $t = 0.66$ (left) and $t = 0.85$ (right) only for the adaptive case since the uniform case has already produced spurious oscillations. We perform the test over different cell numbers $N = 125$, 500, 2000. In the first line, we note that the numerical solutions are clean of oscillations even in high spatial resolutions. In the second line, we see the same graphs as in the first, this time focused on the area of the discontinuity, where we note that the increase of the spatial resolution leads to a sharp limiting profile. In this test the CFL was set to 0.4.

The entropy flux in this case is given by the relation:

$$F'(u) = U'(u)f'(u) \Rightarrow F(u) = \frac{1}{2}u^6.$$

Due to the convexity of the entropy function, we define the new variables, entropy variables v as

$$v(u) = U'(u) \Rightarrow v(u) = u^3 \Rightarrow u(v) = \sqrt[3]{v}.$$

Applying this change of variables we conclude to the new entropy variables:

$$g(v) = f(u(v)) \Rightarrow g(v) = v.$$

The main step now is the construction of the entropy conservative flux $g^*_{i+1/2}$. LeFloch and Rohde (Theorem 3.1) state that the numerical scheme

$$\frac{d}{dt}u_i(t) = -\frac{1}{\Delta x}(g^*_{i+1/2} - g^*_{i-1/2}), \quad g^*_{i+1/2} = g^*(v_{i-1}, v_i, v_{i+1}, v_{i+2}),$$

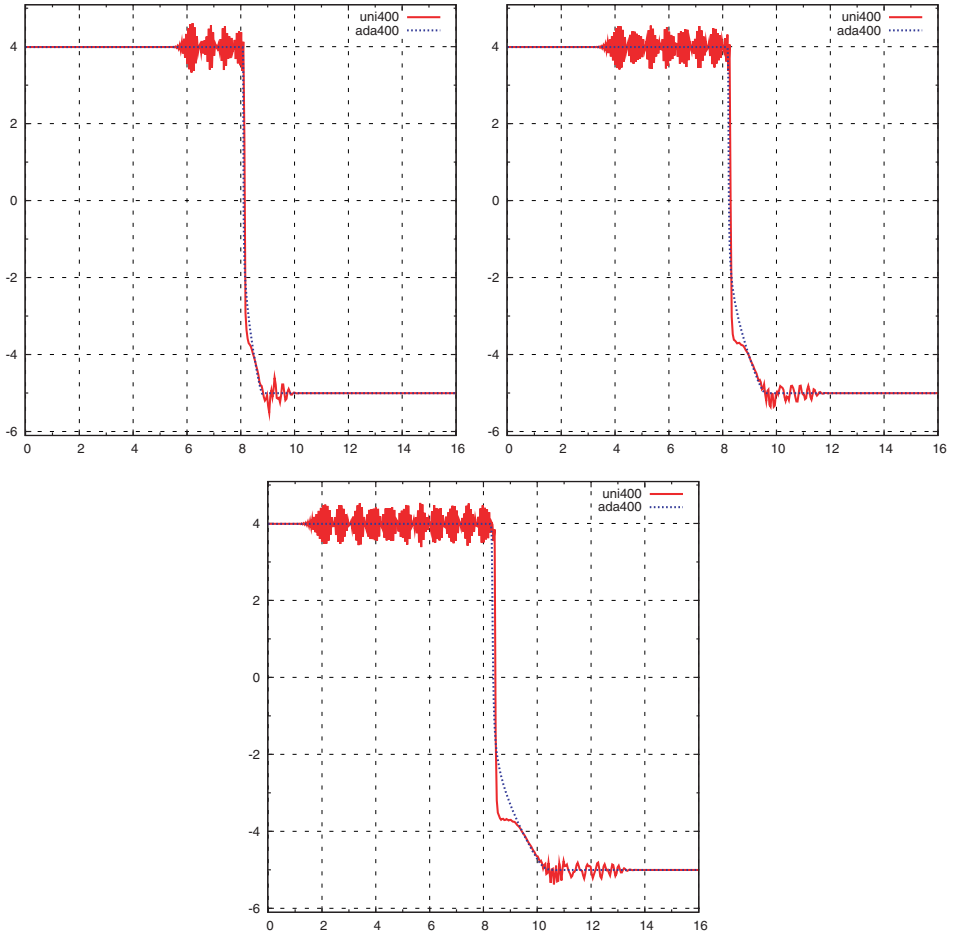

Fig. 7. (Problem 4.) Burgers equation with a jump $u_l = 4$, $u_r = -5$ at $x = 8$ for initial conditions. The pair entropy/entropy flux considered is $(U(u), F(u)) = (\frac{1}{4}u^4, \frac{1}{2}u^6)$. We exhibit times $t = 0.01$ (left), $t = 0.02$ (right), $t = 0.03$ (bottom) for the uniform and the adaptive mesh case. We first note that in the uniform case oscillation appear both at the top and the bottom of the jump. We note that especially in the top the oscillations seem to propagate with a pattern (see Fig. 8), these oscillatory parts are resolved by the adaptive case without any oscillations. Next we note that in the uniform case a plateau created at level $y \approx -3.5$ which the adaptive case does not resolve (see Fig. 8). This test was performed using $N = 400$ cells and 4th order Runge–Kutta temporal discretization of the scheme (4.4).

with entropy conservative flux $g^*(v_{i-1}, v_i, v_{i+1}, v_{i+2})$ defined by

$$g^*(v_{i-1}, v_i, v_{i+1}, v_{i+2}) = \int_0^1 g(v_i + s(v_{i+1} - v_i))ds$$
$$- \frac{1}{12}((v_{i+2} - v_{i+1}) \cdot B^*(v_i, v_{i+1}, v_{i+2})$$
$$- (v_i - v_{i-1}) \cdot B^*(v_{i-1}, v_i, v_{i+1})),$$

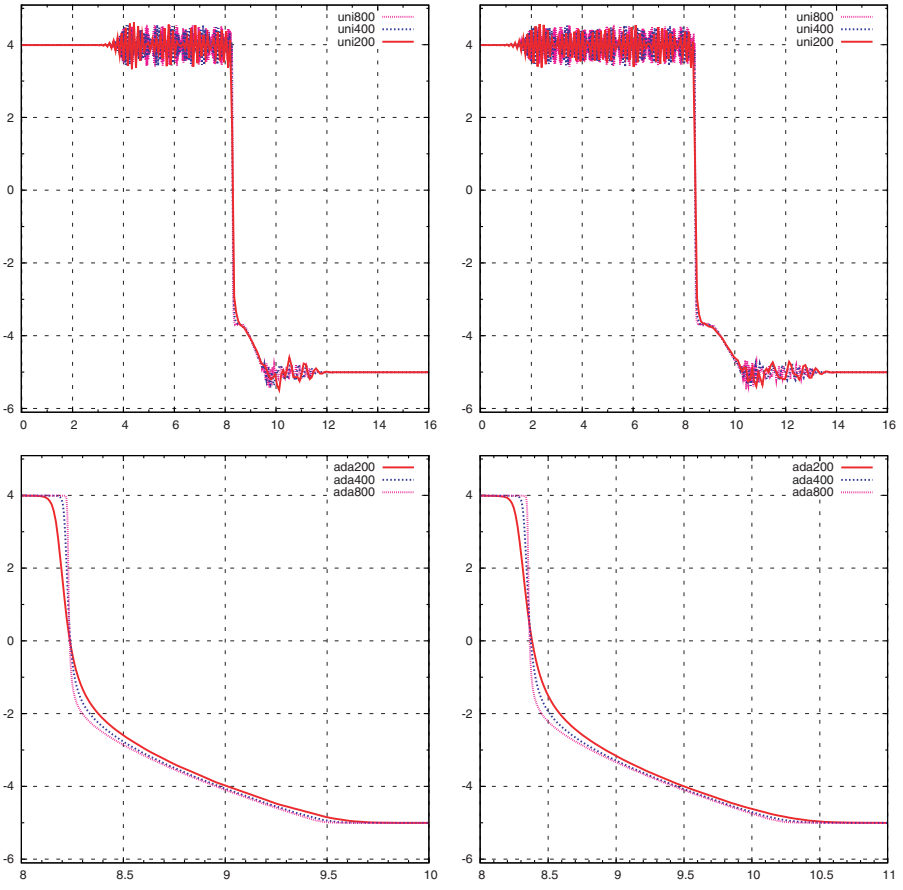

Fig. 8. (Problem 4.) Burgers equation with a jump $u_l = 4$, $u_r = -5$ at $x = 8$ for initial conditions. The pair entropy/entropy flux considered is $(U(u), F(u)) = (\frac{1}{4}u^4, \frac{1}{2}u^6)$. We exhibit times $t = 0.02$ (left) $t = 0.03$ (right) separately for the uniform and the adaptive mesh case over different mesh sizes $N = 200, 400, 800$. In the first line, we present the numerical solutions over uniform meshes and we note that the pattern of oscillations and their frequency varies with N (most notably at the top) while at the same time they keep their speed of propagation. We also note that the creation of the plateau at level $y \approx -3.5$ is persistent with the increase of N revealing that this schemes resolves non-classical shock on uniform meshes. In the second line, we present the area of the jump in the adaptive case. We notice that the results do not exhibit any oscillations and at the same time they converge (as N increases) to a limiting profile that lacks the plateau exhibited in the uniform case. This reveals the failure of the adaptive case to resolve non-classical shocks. These tests where performed after 4th order Runge–Kutta temporal discretization of the scheme (4.4).

is entropy conservative and third order accurate provided,

$$B^*(v,v,v) = B(v) = Dg(v).$$

The choices $B^* = 0$ or $B^* = B$, where $B(v) = Dg(v)$, produce classical shocks, while other choices such as $B^* = 5B$ produce non-classical shocks. We refer to [10] for a thorough discussion on non-classical shocks in conservation laws. We just mention here that these shocks can occur only when the flux function f is not convex, they satisfy a single — instead of the whole set — entropy inequality and they are under-compressive in the sense that characteristics pass through it rather than focus on it.

We finish with the construction of the entropy conservative semi-discrete numerical scheme by selecting $B^* = 5B$, hence the scheme yields:

$$\begin{aligned}\frac{d}{dt}u_i(t) = &-\frac{1}{2\Delta x_i}(g(v_{i+1}) - g(v_{i-1})) \\ &- \frac{5}{12\Delta x_i}(-g(v_{i+2}) + 2g(v_{i+1}) - 2g(v_{i-1}) + g(v_{i-2})).\end{aligned} \tag{4.4}$$

The numerical tests are performed with a Runge–Kutta 4th order temporal discretization and a jump $u_l = 4$, $u_r = -5$ at $x = 8$ initial condition. We refer to Figs. 7 and 8 for graphical representation of the comparison tests of the adaptive case versus the uniform case. Out of the test performed, it is evident that the schemes of [12] when combined with the adaptive mesh selection algorithm of Sec. 2 are transformed to entropy diminishing schemes and they no longer approximate the non-classical shock, but rather the entropy solution of the conservation law.

5. Conclusions

In this work we considered a mesh reconstruction procedure as described in Sec. 2 and we combined it with the entropy conservative schemes of Tadmor for the evolution step of the MAS.

The entropy conservative schemes of Tadmor are designed to serve as building block to construct entropy dissipative schemes for scalar and systems of conservation laws [16]. These schemes constitute an important marginal class for the numerical study of hyperbolic problems. The main conclusions regarding the use of the MAS along with entropy conservative schemes for the time evolution step are:

(1) The entropy conservative schemes, when combined with adaptive mesh selection converge to the entropy solution without oscillations.
(2) Optimal CFL condition can be accomplished even with explicit time discretization.
(3) These schemes are used as a basis for the construction of numerical schemes for non-classical shock computation. Our results show that even in this case these

schemes combined with appropriate mesh selection converge to the entropy solution rather than to the non-classical shock.

It is important therefore to observe the strong stabilization mechanism of mesh selection for this class of schemes. On the other hand, such schemes should be used with care if one wants to compute non-classical shock behavior in non-uniform meshes.

Acknowledgments

Research partially supported by the European Union grant No. MEST-CT-2005-021122 (Differential Equations with Applications in Science and Engineering — DEASE).

References

[1] Ch. Arvanitis and A. Delis, Behavior of finite volume schemes for hyperbolic conservation laws on adaptive redistributed spatial grids, *SIAM J. Sci. Comput.* **28** (2006) 1927–1956.

[2] Ch. Arvanitis, Th. Katsaounis and Ch. Makridakis, Adaptive finite element relaxation schemes for hyperbolic conservation laws, *Math. Model. Anal. Numer.* **35** (2001) 17–33.

[3] Ch. Arvanitis, Ch. Makridakis and A. Tzavaras, Stability and convergence of a class of finite element schemes for hyperbolic systems of conservation laws, *SIAM J. Numer. Anal.* **42** (2004) 1357–1393.

[4] Ch. Arvanitis, Finite elements for hyperbolic conservation laws: New methods and computational techniques, Ph.D. thesis, University of Crete (2002).

[5] Ch. Arvanitis, Mesh redistribution strategies and finite element method schemes for hyperbolic conservation laws, *J. Sci. Computing* **34** (2008) 1–25.

[6] E. Dorfi and L. Drury, Simple adaptive grids for 1d initial value problems, *J. Comput. Phys.* **69** (1987) 175–195.

[7] K. O. Friedrichs and P. D. Lax, Systems of conservation laws with convex extension, *Proc. Nat. Acad. Sci. USA* **68** (1971) 1686–1688.

[8] E. Godlewski and P. A. Raviart, *Hyperbolic Systems of Conservation Laws* (Ellipses, 1990).

[9] A. Harten and J. Hyman, Self adjusting grid methods for one-dimensional hyperbolic conservation laws, *J. Comput. Phys.* **50** (1983) 235–269.

[10] B. T. Hayes and P. LeFloch, Non-classical shocks and kinetic relations: Scalar conservation laws, *Arch. J. Math. Anal.* **139** (1997) 1–56.

[11] A. Kurganov, G. Petrova and B. Popov, Adaptive semidiscrete central-upwind schemes for nonconvex hyperbolic conservation laws, *SIAM J. Sci. Comput.* **29**(6) (2007) 2381–2401 (in electronic).

[12] P. G. LeFloch and Ch. Rohde, High-order schemes, entropy inequalities and non-classical shocks, *J. Numer. Anal. SIAM* (2000) 2023–2060.

[13] M. Lukáčová-Medviďová and E. Tadmor, On the entropy stability of Roe-type finite volume methods, to appear in *Proceedings HYP 2008*.

[14] N. Sfakianakis, Adaptive mesh reconstruction, total variation bound, preprint (2008).

[15] E. Tadmor, The numerical viscosity of entropy stable schemes for systems of conservation laws, *Math. Comput.* (1987) 91–103.

[16] E. Tadmor, Entropy stability theory for difference approximations of nonlinear conservation laws and related time dependent problems, *Acta Numer.* (2003) 451–512.
[17] H. Tang and T. Tang, Adaptive mesh methods for one- and two-dimensional hyperbolic conservation laws, *SIAM J. Numer. Anal.* **41** (2003) 487–515.